doi:10.20944/preprints202209.0449.v1

Article

Numerical Study of the Electromagnetic Field Distribution in Pulsed Power Plasma Stimulation Technique - Potential Feasibility of Underground Detective and Diagnostic Tool

Yue Xiao [1,*], Waylon House [2], Mohamed Y. Soliman [3] and Akif Ibraguimov [2]

[1] Research Institute of Petroleum Exploration and Development (RIPED); 20 Xueyuan Rd; Haidian District, Beijing, 100083, China
[2] Texas Tech University; 2500 Broadway, Lubbock, TX 79409, USA
[3] University of Houston; 5000 Gulf Fwy, Houston, TX 77023, USA
* Correspondence: xiaoyue0324@petrochina.com.cn; Tel.: +86(010)83595965; Cellphone: +86 18561219618

Abstract: The scope of this work was part of our previous research on Pulsed Power Plasma Stimulation Technique. Electromagnetic fields generated during a pulsed power plasma discharge were simulated using a finite element method in the COMSOL RF module. The field distributions were calculated during and after the pulse. The current paper takes advantage of prior work measuring and modeling the current distribution in the plasma arc. Agreement with laboratory experimental measurements provides support for extension of the model to reservoir scale. The validated model was used to quantify the signal attenuation level in different medium environment.

Keywords: pulsed power plasma discharge; electromagnetic; COMSOL; numerical simulation

1. Introduction

Pulsed Power Techniques have been regularly used for rock removal in mining and civil engineering industries as a replacement for more historical techniques. Recently, PAED (Pulsed Arc Electrohydraulic Discharge) and PPPS (Pulsed Power Plasma Stimulation) have been considered as a potential alternative to hydraulic fracturing especially in tight reservoirs and shale formations. Experimental investigations [1]- [5] provide thorough understanding of the fracturing or stimulation mechanism and field trials have already been implemented in mines and oil fields [6].

Associated with the mechanical effects of these techniques are the electrical and magnetic fields produced by the electric arc that generates the plasma. There are electrical and magnetic effects produced by the electric arc that creates the plasma discharge. The possibility exists that these electromagnetic phenomena could provide important real time information during field applications of PPPS. Advanced electromagnetic technologies in detecting mines, voids and other natural barriers [7][8] supports the possibility of using electromagnetic fields for detecting natural boundaries in reservoir like fractures. This study is part of a research program investigating of this possibility.

The field effects of electrical discharge are a widely studied classical topic in electrodynamics. However, no study has been published analyzing the specific situations involved in P3D – an intense electric plasma arc of small dimension and short duration. A pertinent lightning stroke model was proposed by Marcos Rubinstein and Martin A. Uman [1]. The model provided detailed analytical solutions for electromagnetic fields caused by a traveling square-wave current (current duration of μs) using the Vector Potential formalism. One interesting results of their analytical work is that a near magnetic induction zone will form as well as a far electromagnetic radiation zone. The location of these zones depends on the duration of the pulse. It is anticipated that somewhat similar electromagnetic field behavior will obtain with PPPS.

In order to have a preliminary understanding of the electromagnetic phenomenon that occurs as part of our PPPS project, a finite element model for the simulation of electromagnetic behavior was developed using the COMSOL Multiphysics RF module. The model was designed to enable comparison with field measurements on PPPS experiments in our laboratory. A main objective of this paper is to compare the simulation results with a set of scale model experiments in concrete samples. Validating the simulation by comparing it to the laboratory results in the near zone would lead to more confidence in using the simulation to predict EM behavior to distances far greater than possible in laboratory experiments.

2. Model Establishment at Experimental Scale

The experimental samples were cylinders of concrete with a bore tube down the axis of symmetry. The plasma is created in the center of the bore and the magnetic induction is detected by field coils imbedded in the concrete on the central plane near the perimeter of the sample, as shown in Figure 1.

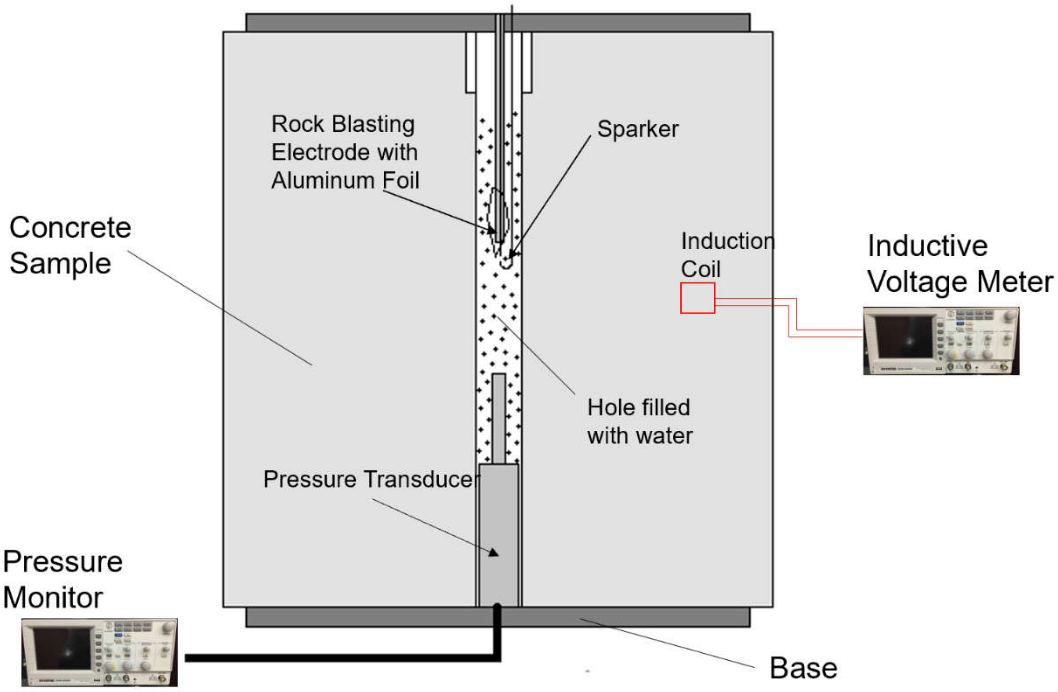

Figure 1. Cross-sectional diagram Vertical well mimicking sample set-ups (Xiao 2017).

3. Model Configuration and Simplification

The simulation domain is a 3-D cylinder with radius of 2 meter and height 3 mete. At the center is the concrete sample. The pulse source (a fusible aluminum link) is located in the center of the sample. The sample is surrounded by air. The dimensions of the concrete sample, borehole size and aluminum link match the experimental situation, see **Table 1** for detail.

The symmetrical characteristics of the physical model make it possible to carry out the simulations in two dimensions on the XY work plane. This 2-D work plane cuts through the center of the 3-D model and is parallel to wellbore, see Figure 2 for more details. The model also uses a physically controlled mesh system with higher grid density at contact surfaces [4], as circled red in lower-right corner of Figure 2.

During the experiments, first, electrical energy is stored in a capacitor over a relatively long time (minutes), and then released in a very short time (μs). The sudden released is accomplished using a spark gap or a fusible link through which the discharge produces a plasma. The ensuing process depends on the media in which the plasma is created (water) and the materials used in the creation of the plasma (Aluminum foil).

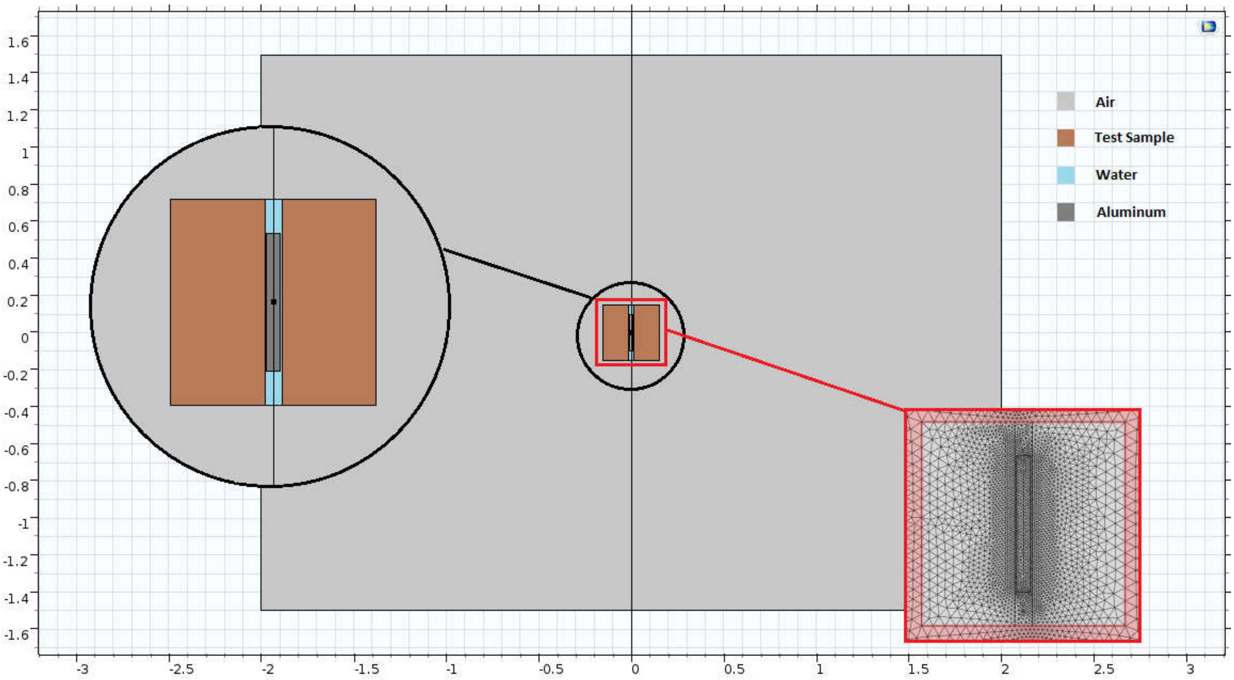

Figure 2. Physical View of Two-Dimensional Work Plane and Physically Controlled Mesh System.

The model uses a physically controlled mesh system with normal element size shown in far field and much smaller element around sample area (Figure 2 lower right red rectangle) where there are more material boundaries. This automatic mesh system creates meshes that are adapted to physics in the model. There is a fine mesh around interior boundaries, at the test sample, the borehole and a coarser mesh for the air domain.

4. Governing Equations and Boundaries Conditions

Governing formulation of transient time model is derived from classical Maxwell's equations under the circumstance of linear, homogenous, isotropic, and time invariant medium.

$$\left\{\begin{matrix}\nabla \times \mu_r^{-1}(\nabla \times \boldsymbol{A}) + \mu_0\sigma\frac{\partial \boldsymbol{A}}{\partial t} + \mu_0\frac{\partial}{\partial t}\left(\epsilon_0\epsilon_r\frac{\partial \boldsymbol{A}}{\partial t}\right) = 0 \\ B = \mu_0\mu_r H\end{matrix}\right\}\dots\dots\dots($$

$\boldsymbol{A}$ − Magnetic Potential Vector, $\frac{\mathrm{wb}}{\mathrm{m}}$, [SI Unit: $\mathrm{V}\cdot\mathrm{s}\cdot\mathrm{m}^{-1}$]

$\frac{\partial \boldsymbol{A}}{\partial t} - First\ Derivative, V/m$

$\boldsymbol{E} - Electric\ Field, V/m$

$\boldsymbol{H} - Magnetic\ field, A/m$

$\boldsymbol{B} - Magnetic\ Induction, T = wb/m^2$

$\mu = \mu_r\mu_0\ is\ the\ magnetic\ permeability, \mu_0 = 4\pi \times 10^{-7}$

σ − electrical conductivity in S/m

$\epsilon = \epsilon_r\epsilon_0\ is\ the\ permittivity.\ \epsilon_0 = \pi/36 \times 10^{-9}\ Fards/meter$

Analytical solutions in general and the inputs to COMSOL require specification of the source surface current and boundary conditions. The arc source can be represented as a transient electric dipole, or as a transient surface current of short arc length. Since the arc current is experimentally measured, this option is appropriate. It is useful to assume scattering boundary conditions to the exterior boundary of the air domain. This condition makes the boundary transparent to the emitted wave allowing projection to infinite distance.

$$\mu_0 \boldsymbol{n} \times \boldsymbol{H} + \frac{\mu_0}{Z_c} \boldsymbol{n} \times (\boldsymbol{E} \times \boldsymbol{n}) - \frac{1/2r + \gamma}{\mu_r} \boldsymbol{n} \times (\boldsymbol{A} \times \boldsymbol{n})$$

$$= \frac{\mu_0}{Z_c} \boldsymbol{n} \times \left(\boldsymbol{E_0} \times (\boldsymbol{n} - \boldsymbol{k_{dir}})\right) - \frac{\gamma}{\mu_r} \boldsymbol{n} \times \left(\boldsymbol{A} \times (\boldsymbol{n} - \boldsymbol{k_{dir}})\right) - \frac{1/2r}{\mu_r} \boldsymbol{n} \times (\boldsymbol{A_0} \times \boldsymbol{n}) \ldots \ldots \ldots ()$$

$$E_0 = -\frac{\partial \boldsymbol{A_0}}{\partial t}$$

$$\nabla \times \boldsymbol{H} = \sigma \boldsymbol{E_0} + \epsilon_0 \frac{\partial}{\partial t} (\epsilon_r \boldsymbol{E_0})$$

$$Z_c = \sqrt{\frac{\mu_0 \mu_r}{\epsilon_0 \epsilon_r}}$$

$$\gamma = \frac{\sigma Z_c}{2}$$

$\boldsymbol{A_0} - Initial\ Value\ for\ Magnetic\ Vector\ Potential, \frac{Wb}{m}$

$r - radial\ coordinate\ of$

$\boldsymbol{k_{dir}} - Incident\ Wave\ Direction, default\ direction\ for\ 2$

$- D\ is\ in\ the\ oppsite\ direction\ to\ the\ boundary\ normal$

The scattered (outgoing) wave types for which the boundary condition is perfectly transparent are

$$\boldsymbol{E} = \boldsymbol{E}_{sc} e^{-jk(\boldsymbol{n}\cdot\boldsymbol{r})} + \boldsymbol{E}_0 e^{-jk(\boldsymbol{K}\cdot\boldsymbol{r})} (incident\ wave) \qquad \text{Plane Scattered Wave}$$

$$\boldsymbol{E} = \boldsymbol{E}_{sc} \frac{e^{-jk(\boldsymbol{n}\cdot\boldsymbol{r})}}{\sqrt{r}} + \boldsymbol{E}_0 e^{-jk(\boldsymbol{K}\cdot\boldsymbol{r})} \qquad \text{Cylindrical Scattered Wave}$$

$$\boldsymbol{E} = \boldsymbol{E}_{sc} \frac{e^{-jk(\boldsymbol{n}\cdot\boldsymbol{r})}}{r_s} + \boldsymbol{E}_0 e^{-jk(\boldsymbol{K}\cdot\boldsymbol{r})} \qquad \text{Spherical Scattered Wave}$$

$\boldsymbol{E}_0 - incident\ plane\ wave\ that\ travels\ in\ the\ direction\ of\ \boldsymbol{k}$

The boundary condition is transparent for incoming (but not outgoing) plane waves with any angle of incidence.

5. Arc Source Current

The experimentally measured current flow through the arc discharge is shown in **Figure 3**, with a peak value of around 35 kA. The source term of the numerical model can be formulated as a simple damped exponential analytical waveform shown as below:

$$I(t) = 45e^{-0.04t} \cos\left(\frac{\omega_0}{2 \times 10^6} t - \frac{\pi}{2}\right) 0 < t < 50\ \mu s$$

$$\omega_0 = \frac{2\pi}{\tau_0} = \frac{2\pi}{12.5 \times 10^{-6} s} = 502654\ Hz$$

doi:10.20944/preprints202209.0449.v1

The analytical current equation was imbedded input to COMSOL RF module and will be used to generate the source current density. The equation below specifies the source current density

$$\boldsymbol{n} \times \boldsymbol{H} = \boldsymbol{J_s}$$

n – normal component vector

$\boldsymbol{J_s}$ – $Surface\ Current\ Density, A/m$

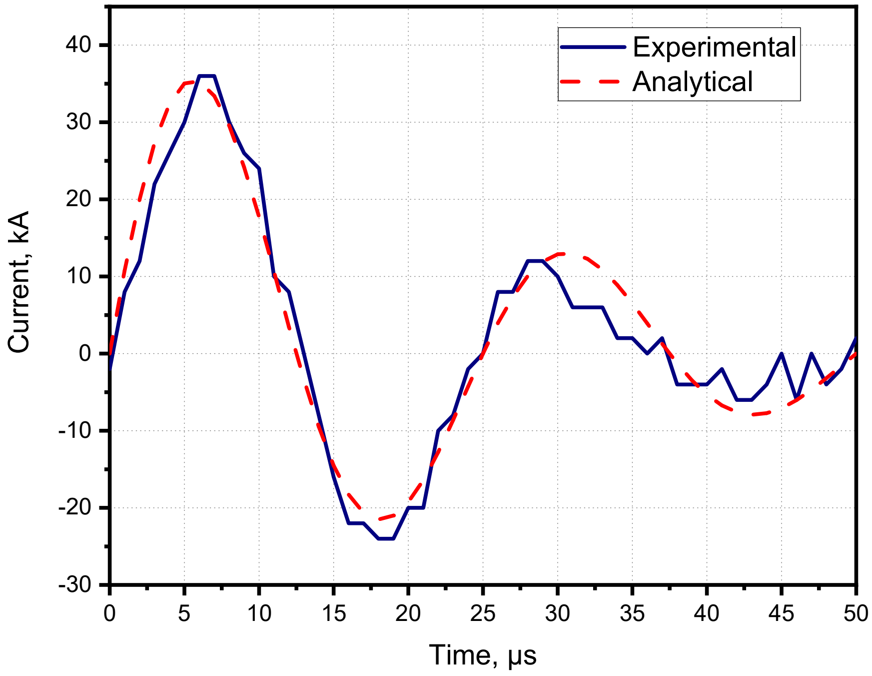

Figure 3. Time Profile of Measured Current.

6. Material Properties

All the material properties were imported directly from the COMSOL library except for dielectric constants. The dielectric properties of rock were averaged from shale rock data [9]. **Table 2** lists the three significant dielectric constants that need additional assignments as well as their relationship with electromagnetic parameters.

Table 1. Materials and Dimensions.

Material	Domain Radius(m)	Domain Height (m)
Air	2	3
Aluminum-foil	0.01	0.2
Water	0.0177(w=1in.)	0.3
Rock	0.3	0.3

Table 2. Equations Defining Dielectric Properties.

EQUATIONS	
$\boldsymbol{D} = \epsilon \mathbf{E}$	$\boldsymbol{D} - electrical\ displacement, coulomb/m^2$ $\boldsymbol{E} - electric\ field\ intensity, V/m$ ϵ − relative permittivity
$\boldsymbol{J} = \sigma \boldsymbol{E}$	$\boldsymbol{J} - electric\ current\ density, A/m^2$ $\sigma - electrical\ conductivity$
$\boldsymbol{B} = \mu \boldsymbol{H}$	$\boldsymbol{B} - magnetic\ induction, weber/m^2$ $\boldsymbol{H} - magnetic\ field\ intensity, A/m$ $\mu - relative\ magnetic\ permeability$

The material in the simulation plane consists of air, rock and water in the borehole, as well as aluminum. The properties of air, water, and aluminum are readily available (**Table 3**). In comparison, the properties of reservoir rocks range widely because of heterogeneity and complex composition. Typical values of shale reservoir non-magnetic rock are summarized in **Table 4** from a previous work

Table 3. Material Properties.

Properties	μ_r	σ	ϵ_r
Water	1	5.5×10^{-6}	80
Aluminum	1	3.774×10^{7}	1.8
Air	1	8×10^{-15}	1

Table 4. Material Properties of Rock

Properties	Symbol	Value	Unit
Relative Magnetic Permeability	μ_r	10(non-magnetic)	None
Electrical Conductivity	σ	0.0001	S/m
Relative Permittivity	ϵ_r	4.5	None

7. Simulation Results and Discussion

Time derivatives of Magnetic Fields dB/dt

The PPPS technique in 3-D is modeled as a transient line segment current with the current direction specifying the axial direction. In both cylindrical and spherical coordinate systems, the created B field in homogeneous media would be in the angular (ϕ) direction. In the 2-D representation considered here, the magnetic field shows a Z component. By cylindrical symmetry, the same value of B will obtain at any point normal to the 2-D work plane provided it is at the same distance from the source

As will be discussed later, the time derivatives of the generated magnetic fields are of central importance. In near field applications, the techniques available to practically measure and detect the electromagnetic fields in the near zone will depend on the induced EMF in search coils that depend on d**B**/dt. The simulation results shown below (**Figure 4** to **Figure 6**) will be used to compare with the d**B**/dt experimental data. Note the declining amplitudes with time as well as the oscillation in field strength that is consistent with the current source time behavior.

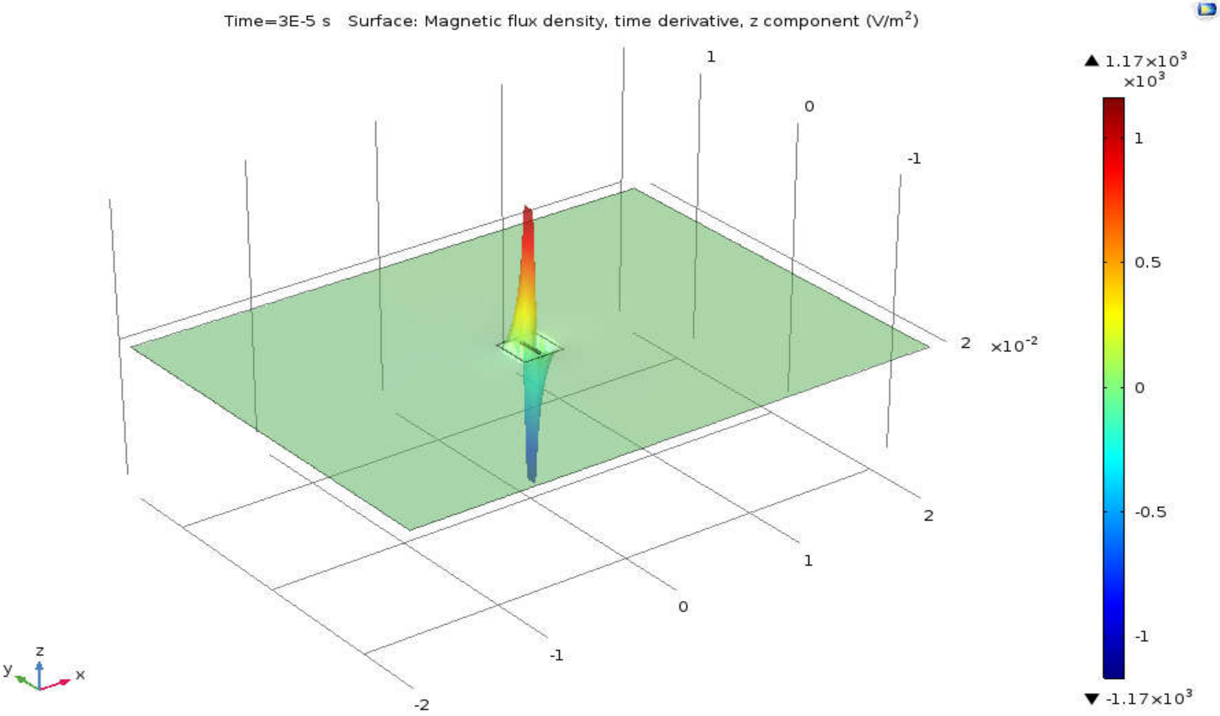

Figure 4. Magnetic Flux Density, time derivative, 3-D View with Height Expression, V/m2.

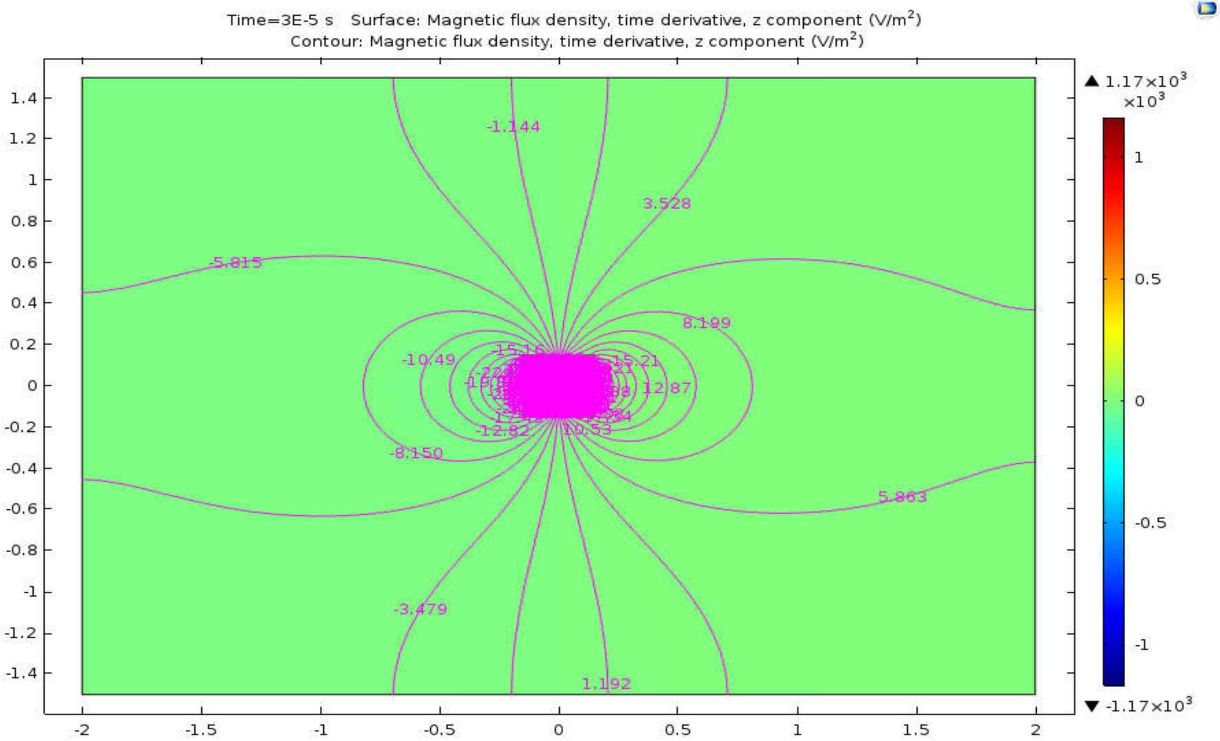

Figure 5. Time derivative of Magnetic Flux Density **B**, 2 D Contour Surface, V/m$^{2.}$

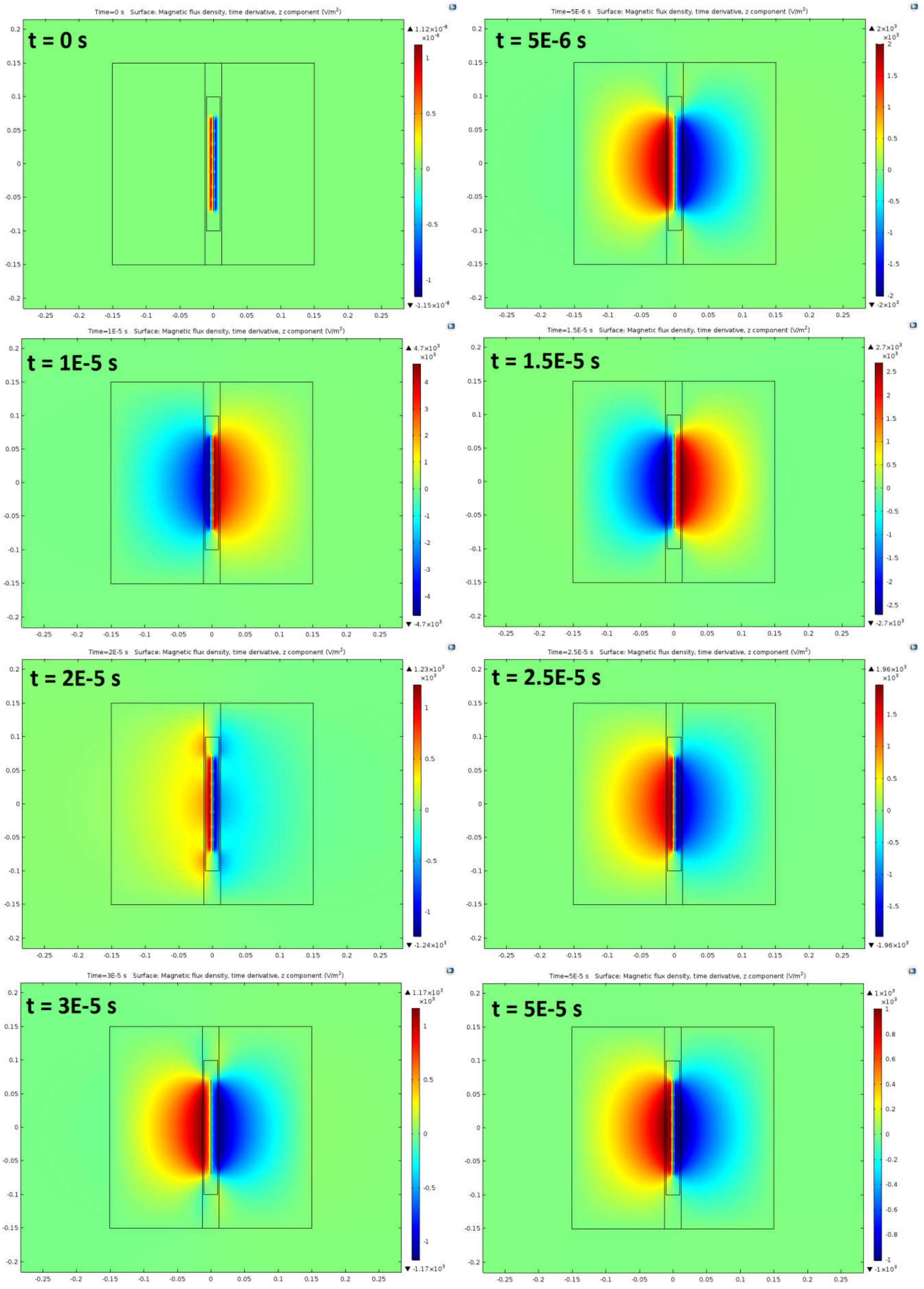

Figure 6. Time Derivative of Magnetic Flux Density, d**B**/dt V/m2.

Experimental Results Match – NEAR ZONE

Table 5 list all the available magnetic data acquired from experimental data, analytical representation, and simulated results, "-" means no direct data can be achieved. In simulation model, analytical representation of the measure current data is used as input surface current density data. An interesting interference between the induced voltage meter and the pressure transduced was captured by the DSO at the burst of the main pressure pulse, shown in **Figure 7**. The transient glitch in the induced EMF at 12 μs is believed to be due to modulation of the plasma current by the creation of the secondary shockwave as seen in the pressure record. This unusual discontinuity is not modeled by the simulation and is ignored in comparing the simulated near field d**B**/dt with the experimental measurements.

Observation point selected in simulation model is on test sample boundary where induction coil was placed during experiments, location is shown in **Figure 8**. The experimental results are detailed in **Figure 9** as the inductive voltage generated by the current.

Table 5. Data Acquirement

	Symbol	Experimental	Analytical	Simulated
Current	**I**	A	A	A
Magnetic Flux Density	**B**	-	-	A/m
Magnetic Field Norm	**H**	-	-	A/m
Current Time Derivative	**dI/dt**	-	A/s	-
Magnetic Flux Density, time derivative	**dB/dt**	V/m^2	V/m^2	V/m^2
Inductive Voltage	**EMF**	V	-	-

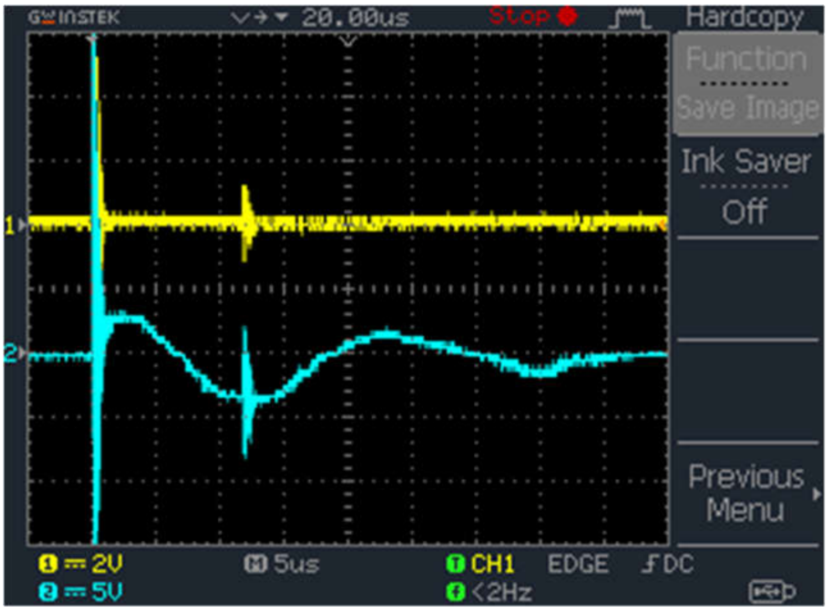

Figure 7. Experimental Pressure data (YELLOW) and EMF (BLUE) data Recorded by DSO 2.

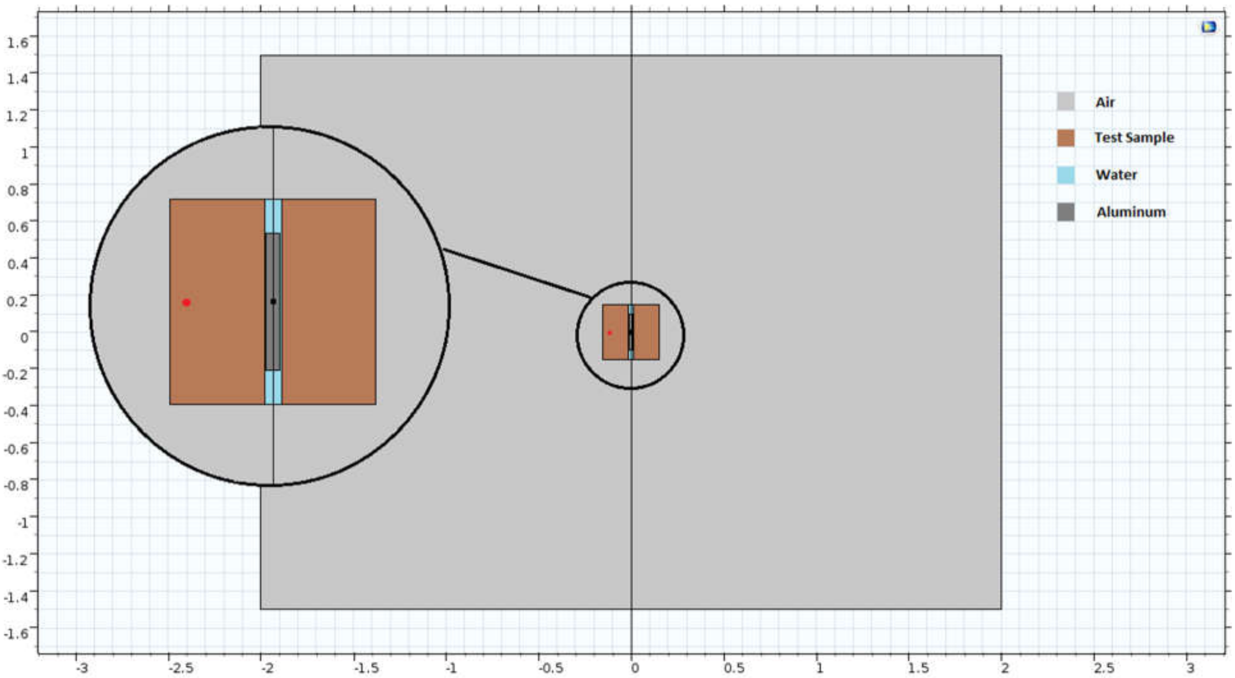

Figure 8. Location Observation Point to be matched with Experimental Data.

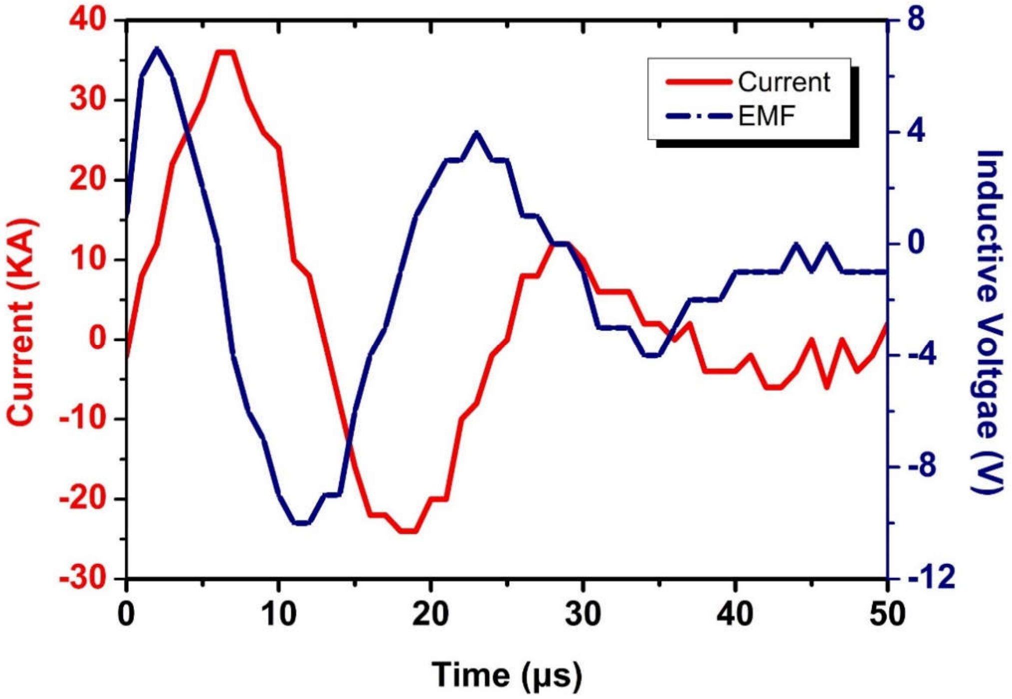

Figure 9. Experimental Current, kA and Inductive Voltage, V.

Also shown are the results of an analytical calculation made possible by placing the EMF detection coil in the plane of symmetry. Good agreement (Figure 10) is obtained which lends support for use of the simulation beyond the near zone to intermediate and far radiation zone as well as differing media properties

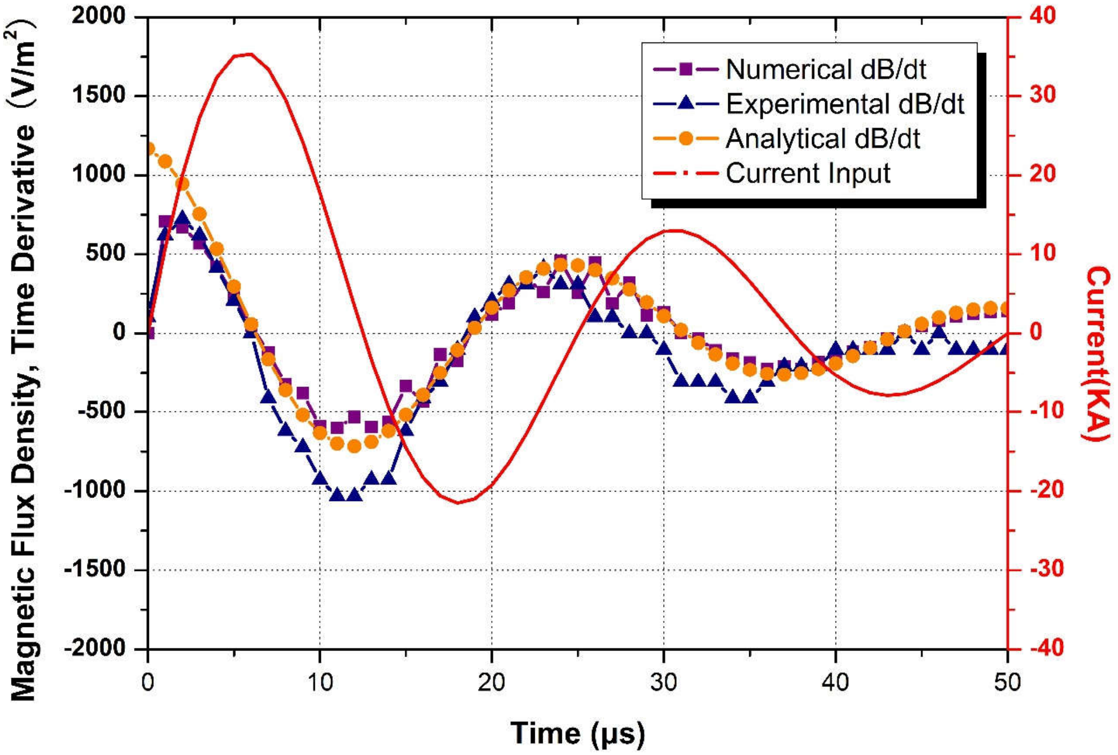

Figure 10. Surface Current Density, Simulated dB/dt, Experimental dB/dt, and Analytical dB/dt.

Comparisons of Cases with Different Surrounding (Air, Water, and Rock)

During the experiments, test samples are exposed in air surrounding. As has been shown in the evaluation section 6.3, the strength of magnetic field and decays very fast in air domain away from the current source and thus the time derivative d**B**/dt signal. This can be explained by the dielectric properties of air.

Another two parallel models are built by replacing the exterior domain of air with water and rock. The objective of this parallel comparison is to provide basic visualization of how electromagnetic waves behave to distinguished materials. **Table 6** lists the dielectric properties of water, rock, and air and **Table 7** is the numerical results of field strength range at T = 0.00003 s. The maximum and minimum strength of dB/dt, magnetic field, and electric field are listed. **Figure 11** to **Figure 13** are the summarized point evaluation and cutline evaluation of these three models.

Table 6. Dielectric Properties of Materials

Properties	μ_r	σ	ϵ_r
Water	1	5.5×10^{-6}	80
Rock	10	1×10^{-5}	4.5
Air	1	8×10^{-15}	1

Table 7. Field Strength of Compared Model of Test Sample Exposed to Air, Water, and Rock.

	dB/dt, V/m²		H, A/m		E, V/m	
	Max	Min	Max	Min	Max	Min
Water	517	-517	6.59×10^3	2.28×10^{-3}	4.24×10^{10}	268
Rock	805	-805	6.61×10^3	5.47×10^{-3}	4.25×10^{10}	190
Air	1.17×10^3	-1.17×10^3	6.62×10^3	2.02×10^{-4}	4.3×10^{10}	34.6

In **Figure 14**, it can be seen that the inductive signal is almost three times stronger for water, rock model during the first positive phase ($0 < t < 7$ μs). For the rest of the simulation time from 7 μs to 50 μs, the difference of signal strength becomes smaller with the time. Even though these three inductive signals have quite similar waveform, it is obvious that the water signal has phase shift and comes 2 μs ahead of time compared with other two. Phase shift has also been detected at other selected evaluation points. In **Figure 12** for horizontal direction and Figure 13 in vertical direction, as for the resultant magnetic field **H**, it can be concluded: as the distance away from the source point increased, the strength of magnetic field becomes weaker and changing much faster than the original current source. This decay is more obvious in air model than in water model. However, this phenomenon is partially true expect that the oscillating pace of the resultant magnetic field remains the same for all observation points.

Figure 14 are the 2-D surface of dB/dt and H of three model simulation results. By referring to Figure 14 and Figure 15 at the same time, it is found that air domain “absorbs” the electromagnetic energy which make the inductive signal much weaker to be detected. Comparisons of models on horizontal cutline and vertical cutline have proved the directional behavior of magnetic field generated by line source current. This is an important guidance for the location of signal receiver in future field test. Signal could be almost undetectable in parallel direction of the current. As seen in the semi-log plot Figure 12, magnetic field decays very fast away from the source and reaches below the magnitude of 0.01 A/m within several meters of distance in spite of the surrounding materials. On the other hand, the evaluation on the perpendicular direction of the source current shown in Figure 13 illustrates that the main decay of magnetic field strength occurs within the rock for air model. The decay of magnetic field is following the same pattern as indicated by the parallel curve in the semi-log plot.

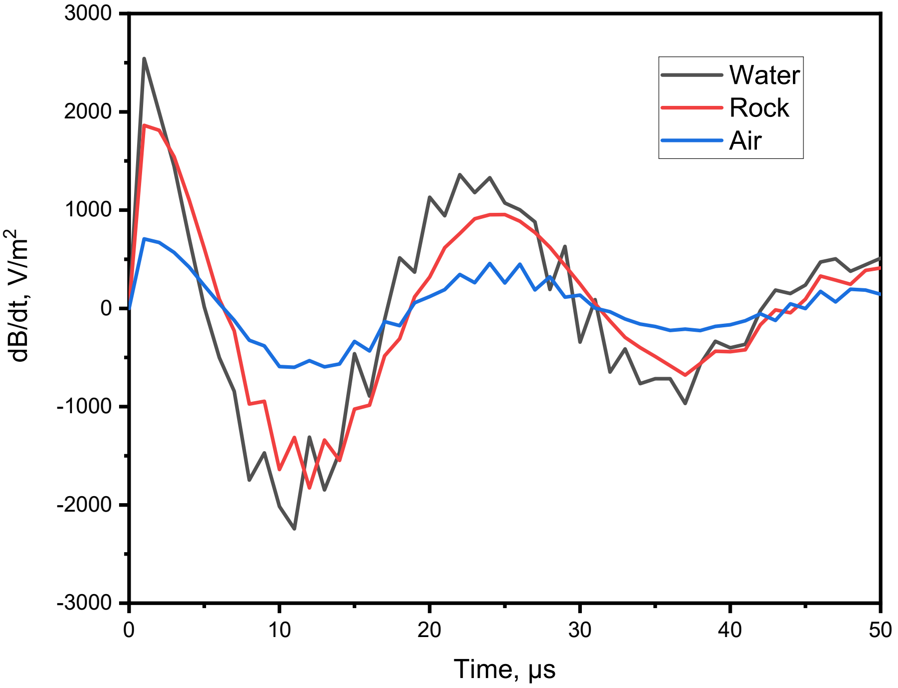

Figure 11. Evaluation at the Selected Matching Point.

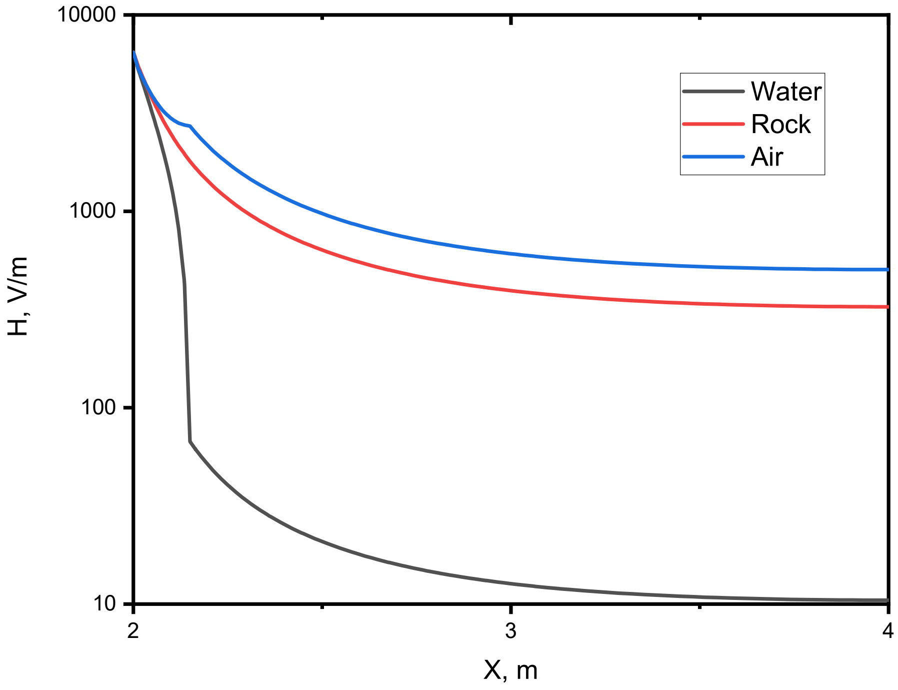

Figure 12. Semi-log Plot of Magnetic Field **H**, V/m², Evaluation on **Horizontal Middle Cutline.**

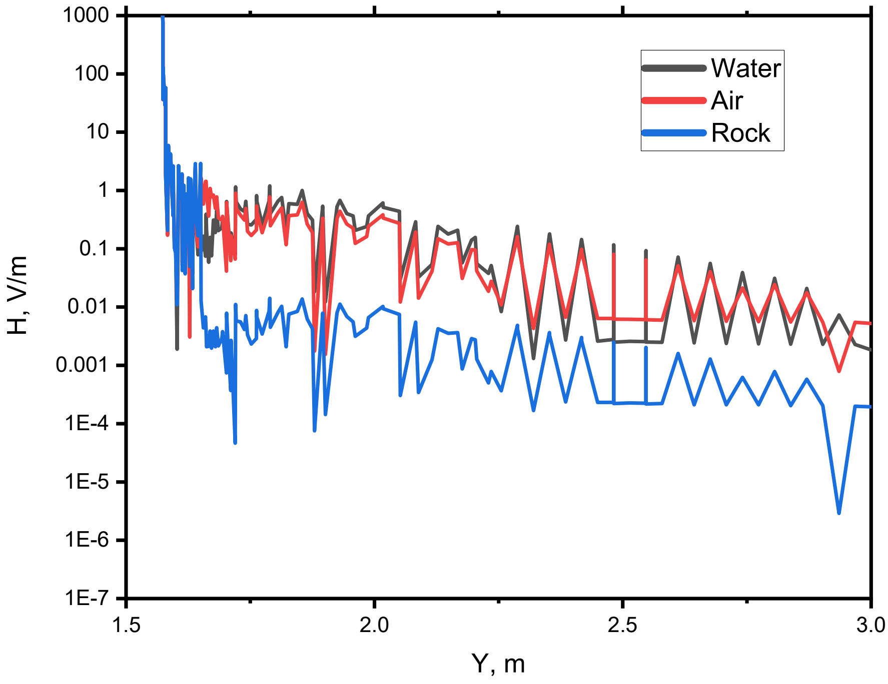

Figure 13. Semi-log Plot of Magnetic Field **H**, V/m², Evaluation on **Vertical Middle Cutline.**

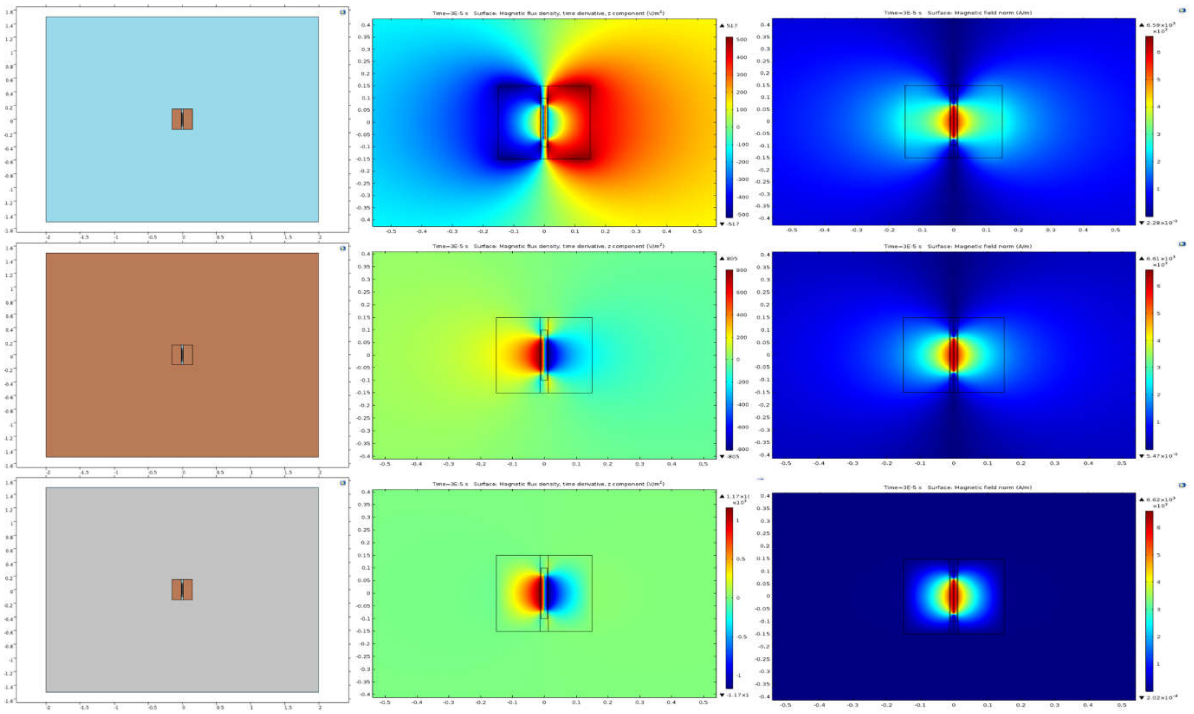

Figure 14. Magnetic Flux Density, Time Derivative d**B**/dt(V/m^2) and Magnetic Field, **H**(A/m).

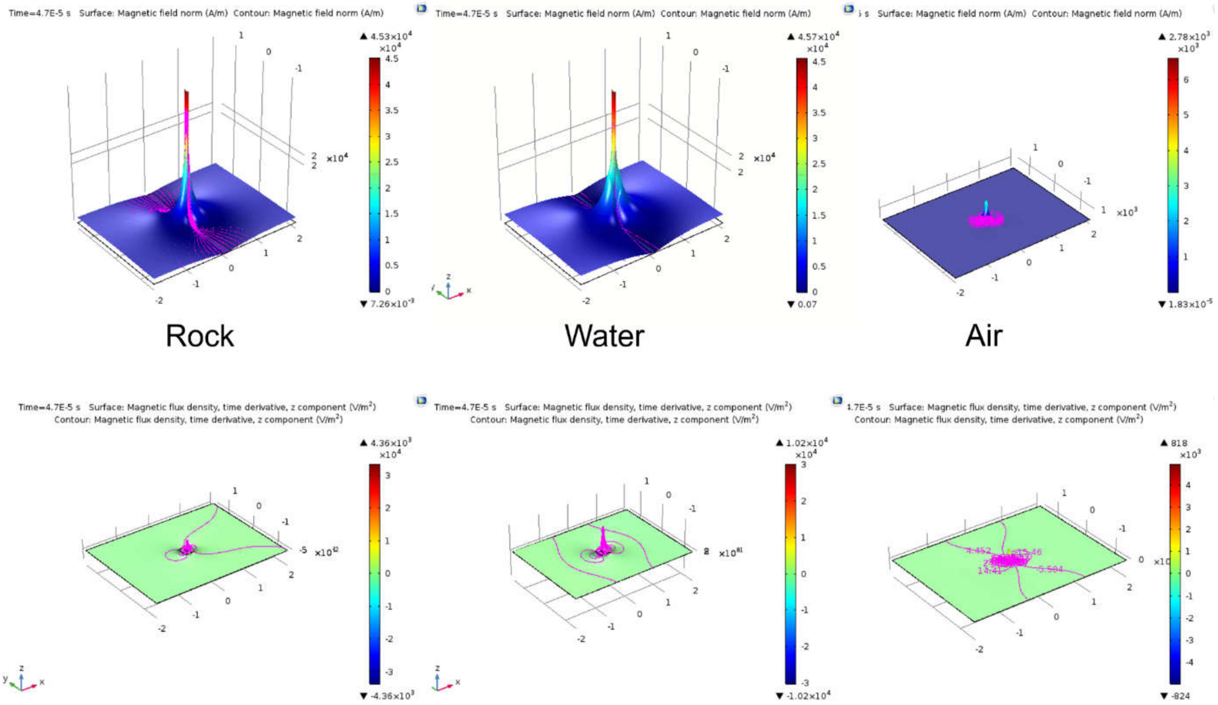

Figure 15. Electrohydraulic Fracturing of Rocks, 1st Edn. John Wiley and Sons Inc., New Jersey, USA, ISBN: 978-1-84821-710-2.

8. Discussion & Conclusions

A numerical model based on the Vector Potential Formalism has been developed in COMSOL Radio Frequency Module. The model was successfully validated in the near zone by matching with experimental results obtained with search coils in laboratory works using the experimental current input. Extension of the model to intermediate and far zone regions is planned to determine feasibility of using this phenomenon in field level applications.

Considering reservoir underground circumstances and the fact that electromagnetic behavior is strongly depends on rock properties especially the fluids inside the pore, comparisons among common reservoir environments were made to investigate the quantitative attenuation of the electromagnetic signal for the lab scale work. The simulation comparisons among the real experimental environment(air) and the other two circumspective rock and liquid were made while maintain all the rest of the conditions the same. The results showed that air surrounding diminish the induction signal strength while liquid surrounding amplify the signal strength by providing more conductive environment. It is also manifested in the semi-log plot that liquid(water) surrounding dampens the magnetic field in X direction for more than ten magnitudes inside the sample volume.

The experimental-validated model would provide confidence for extended field scale simulation work, and establish a workflow for potential feasibility of the Pulsed Power Plasma technique as an underground imaging tool, to be as a cost-effective alternative or substitute for current low accuracy Microseismic technology.

References

1. Zhou, Haibin, Zhang, Yongmin, and, Li, Hengle, 2015"Generation of Electrohydraulic Shock Waves by Plasma-Ignited Energetic Materials: I. Fundamental Mechanisms and Processes", IEEE TRANSACTIONS ON PLASMA SCIENCE **43** (12): 3999-4008
2. Mao, R., De Pater, H. J., Leon, J. F., Fram, J. H., Ewy, R. T., Storslett, S., & Stefani, J. 2012. Experiments on Pulse Power Fracturing. Presented at the SPE Western Regional, Bakersfield, California, 19-23 March 2012. SPE 153805.
3. Xiao, Y., House, W., Unal, E., and Soliman, M.Y., "Pulsed Power Plasm Stimulation Technique – Experimental Study on Single Pulse Test for Fractures Initiation", Hydraulic Fracturing Journal,**4**(3)67-74, July (2017).
4. Xiao, Y., House, W., Soliman, M.Y., "Pulsed Power Plasma Stimulation Technique – Experimental Study on Single Pulse Test for Fracture Initiation", presented at the Unconventional Resources Technology Conference held in Houston, Texas, USA, 23-25 July, 2018, URTeC 2881050, (2018)
5. Zhang, Y.M., Meng, Z., Qin, Y., et al., Innovative Engineering Practice of Soft Coal Seam Permeability Enhancement by Controllable Shock Wave for Mine Gas Extraction: A Case of Zhongjing Mine, Sichuan, Guizhou Province,China[J]., Journal of Coal Society, 44(8): 2388-2400, (2019)
6. Larry G. Stolarczyk, Syd S. Peng, "*Advanced Electromagnetic Wave Technologies for the Detection of Abandoned Mine Entries and Delineation of Barrier Pillars*", presented to Mine Safety and Health Administration (MSHA) and Office of Surface Mining Reclamation and Enforcement (OSMRE), Interactive Forum on Geophysical Technologies for Detecting Underground Coal Mine Voids, July 28-30,2003, Lexington, Kentucky
7. Larry G. Stolarczyk, Robert Troublefield, James Battis, 2005 "Detection of Underground Tunnels with Synchronized Electromagnetic Wave Gradiometer", Proc. Of SPIE, **5778**: (994-1001), DOI: 10.1117/12.609623.
8. Alex Martinez and Alan P. Byrnes, *2001.* "Modeling Dielectric-constant Values of Geologic Materials: An Aid to Ground Penetrating Radar Data Collection and Interpretation", *Current Research in Earth Sciences, Bulletin 247, part 1. (http://www.kgs.ukans.edu/Current/2001/martinez/martinez1.hmtl)*